Bachelor Research Project

Analysis of ion energies by means of a Retarding Field Analyzer and a first application to charge exchange in He^{2+}-H_2 collisions.

Author :
Rutger Haan
S3602885

First Examiner/Supervisor:
Prof. dr. ir. R. Hoekstra
Second Examiner:
dr. T. Schlathölter
Daily Supervisor:
K. I. Bijlsma, MSc

May 30, 2022

university of groningen

faculty of science and engineering

Abstract

In this thesis the question whether compact retarding field analyzers can be used to measure ion energy distributions, was explored. Experiments have been performed where the mean current was measured as a function of the voltage on the retarding grids of the Retarding Field Analyzer (RFA), on the ions 4 keV H^+, 8 keV He^{2+} and 12 keV Sn^{3+}. Moreover, first charge exchange measurements were performed for the He^{2+} in the presence of 1 mL min^{-1} flow of H_2 gas. These measurements were performed in order to determine the resolution of the RFA as well as measure the percentage of He^{2+} that absorbed an electron from the H_2 gas. The resolution of the RFA resulting from the H^+ experiments was found to be 1.03 $\pm$ 0.10%, the He^{2+} experiments were found to be 1.26 $\pm$ 0.06%. The He^+ ions, produced by charge exchange, showed a resolution of 2.21 $\pm$ 0.35%, the apparent reduction of the resolution might be due to some broadening of the ion's stemming from their charge changing collisions with H_2 . Furthermore, when the currents of He^{2+} and He^+ were compared, the percentage of He^{2+} ions that reacted with H_2 gas could be determined. It was found that 2.53 $\pm$ 0.02% of He^{2+} ions have exchanged their charge with H_2 gas. Lastly, the resolution of the RFA was calculated from the Sn^{3+} experiments. It was found that the resolution was 0.98 $\pm$ 0.19%. The resolutions resulting from the different ions are in good agreement with each other and thus boosts the confidence in a 'true' resolution of the RFA, that is found to be around 1%.

Contents

1 Introduction

Ions are present everywhere in nature, from the minerals in your body to the different substances in the oceans. It is no surprise that ionic interactions play a key role in various physical and chemical processes. One of these ionic interactions is charge exchange, i.e. the exchange of electrons between two or more charged particles. In this thesis we explore the exchange of charges between energetic Sn^{3+} ions and H_2 gas with the use of a Retarding Field Analyzer (RFA).

Ever since the invention of the vacuum tube [1], scientists have tried to create a better working alternative for these noisy, energy consuming amplifiers to amplify voltages inside electrical circuits. On the 26th of January 1954, Morris Tanenbaum created the first working silicon transistor [2]. A transistor is a device that can change its conductivity based on a voltage that is applied to the gate of the device. This makes for a precise switch or amplifier based on the input voltage and voltage applied to the gate. An overview of a transistor is depicted in fig. 1.

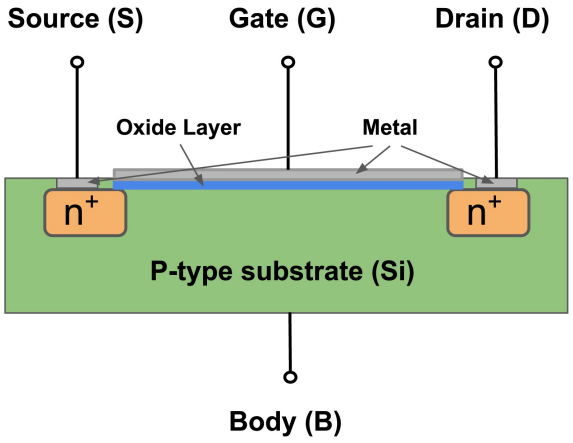

Figure 1: A crossection of a metal–oxide–semiconductor field-effect transistor (MOSFET) [3]. 4 Distinctive components can be identified inside the MOSFET. On the left side we have the Source, where the input voltage is connected to. When a bias is applied, the electrons flow from the Source to the Drain proportionate to the bias applied on the gate. One can see that if a bias on the gate is equal to the bias on the Source, the transistor acts like a switch. However when a greater bias is applied than the input voltage, the transistor acts like an amplifier. The Body terminal is connected to ground.

The transistor can be seen as the basis component of almost all electrical circuits that exist on Earth. This also holds for electronic devices like computers and smartphones, where the amount of transistors in components like the Central Processing Unit (CPU) and Graphical Processing Unit (GPU) determine the processing capacity. As these devices require certain dimensions to be practical and user friendly, the only way to increase the performance of these devices is to make smaller computer chips. The production of smaller computer chips is intertwined with the fabrication of smaller transistors. There is an empirical law by Gordon Moore, called Moore's Law, that states that the amount of affordable transistors on an integrated circuit doubles about every two years [4]. Over the past decades the transistor count per chip have increased from about 2000 in 1970 to about 50 billion in 2020. That is an incredible increase of 25 million times. To be able to produce 50 billion transistors on a single computer chip, one can imagine that you need very precise and accurate nanolithographic machines that can make these computer chips. These nanolithographic machines can etch the transistors on a silicon wafer with nanometer precision. The newest chip machine of ASML can print computer chips with EUV light of 13.5 nm in wavelength [5].

To produce this EUV light a tin droplet is irradiated with a laser pulse and gets so hot that a tin plasma forms that also emits the EUV light. A mirror then collects the produced 13.5 nm EUV light and redirects the beam to the desired lithography tool. However during the impact on the tin droplet, tin ions are produced with a broad range of charge states. These tin ions might impact on the mirror which would degrade the mirror quickly, the costs to keep the machine in operation would therefore increase tremendously. In order to extend the lifetime of the mirror, hydrogen gas is present in the plasma chamber to slow down the tin ions and thereby prevent the degradation of the mirror. Unfortunately, little is known about why hydrogen gas is so great for slowing down and mitigating tin ions. This thesis focuses on exploring the energy transfer that is involved in charge exchange collisions with H_2 with the use of an RFA. An RFA is a device that can measure the current produced by incoming ions, but can also control the amount of ions that impact the device via several grids. On the retarding grids in the RFA, a bias can be applied, of max. 5 kV, to create an electric field between the retarding grids and the grounding grid. On increasing the retarding voltage, the ions will experience lensing effects by the grids until the retarding voltage matches the potential of the ions and the ions will be blocked entirely. Due to imperfections in the RFA itself, the blocking of incoming ions is not realised immediately. There is an offset in the voltage at which the ions will all be blocked out. If we measure this offset, we can calculate the convoluted resolution of the RFA and the ions. By including charge exchange with H_2 gas, we can find out the percentage of ions that have reacted and the change in offset between the different charge states of the ion. In this thesis the H^+, He^{2+} and Sn^{3+} ions have been used for the transmission spectrum measurements. He^{2+} ions have been used to perform the charge exchange measurements. An image of an RFA mounted on a flange can be seen in fig. 2. A flange is a cap that can hold a measuring device and can be mounted on an Ultra High Vacuum (UHV) system, so the vacuum inside can be contained.

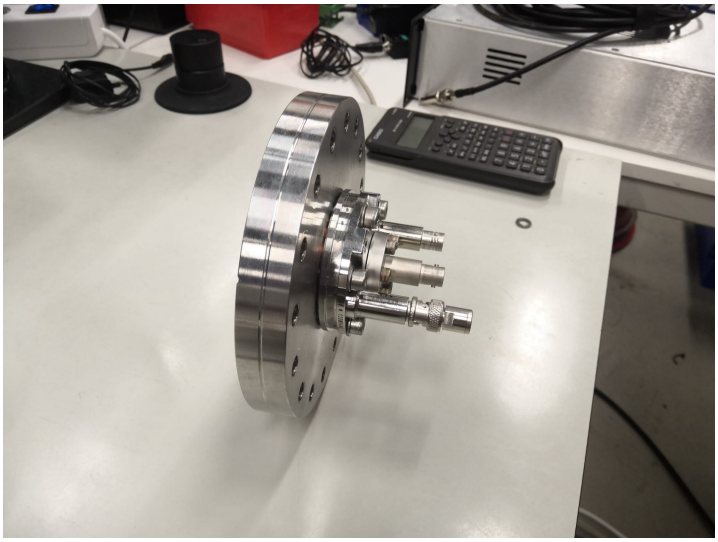

Figure 2: An RFA mounted on a flange. The RFA has three inputs: One for the ground (middle connector), one for the suppression grid (shortest connector) and one for the retarding grids (longest connector).

2 Theoretical Background

This section presents the theoretical background for this thesis. To answer the question: "Can Compact Retarding Field Analyzers be used to measure ion energy distributions ?", an understanding of the underlying principles is necessary. These principles will be explained in the different subsections below.

2.1 Electric fields

One of the most important aspects of the working of an RFA are the electric fields and biases that are created by the voltages put on the different grids [6, 7]. An electric field is created when (a) positive and negative charge(s) are in proximity of each other and their interaction forms a field inbetween them. The equation for the electric field is given by eq. (2.1).

$$\mathbf{E} = -\nabla V \tag{2.1}$$

Where E is the electric field in (V/m), ∇ the vector differential operator and V the potential in (V). This equation can then be used to calculate the electric field strength that determines how the ions can travel through the grid. The way incoming ions are influenced by the potentials on the different grids, has been illustrated in fig. 3.

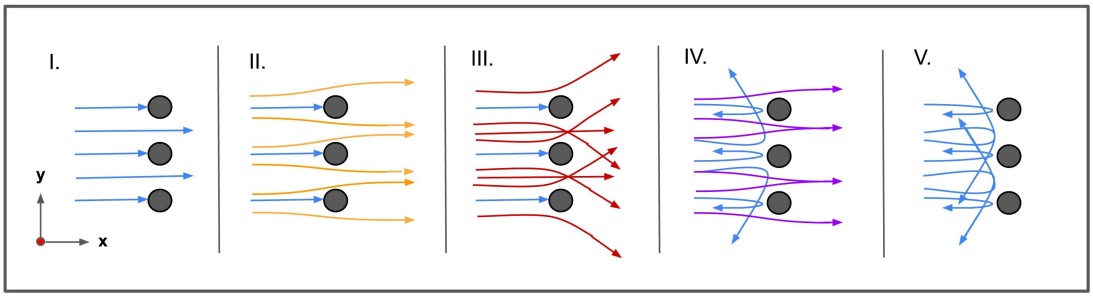

Figure 3: According to [6], there are different situations where the potential on the grids (filled circles) influence the incoming ions (arrows to the right). I) Here there is no or a very small potential on the grid compared to the ion energy. II) There is now a significant potential on the grid such that the converging lensing effect becomes apparent. III) Here part of the incoming ions are now being deflected by the potential on the grids. IV) The lensing effect is now so strong that the ions are strongly focussed in the middle of the grid. V) perfect reflection of all incoming ions, because the potential on the grids is now higher than the energy of the incoming beam.

The influence of the retarding potential on the grids can be plotted against the ion current measured by the Faraday cup of the RFA. The ion current as a function of the potential on the retarding grids can be seen in fig. 4

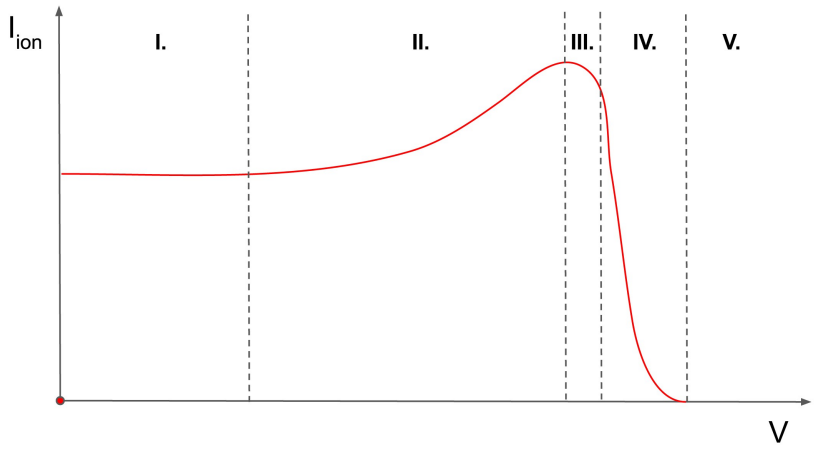

Figure 4: The ion spectrum that corresponds to the regions mentioned in fig. 3, according to [6].

The electric field can then be used to slow down incoming ions to the point where they are entirely retarded so they can not reach the Faraday cup. This can be obtained by setting a potential on the retarding grids that is equal or greater than the potential corresponding to the incoming beam energy, i.e. the potential at which the ions were created. If the current is read out at the Faraday cup, the resolution of the RFA can be determined.

2.2 Charge Exchange

Charge exchange is an important aspect of the measurements that were performed. Charge exchange is the exchange of electrons between different ions or neutral particles, such that their charge states changes after the interaction [8–12]. An illustration of a charge exchange interaction is shown in fig. 5.

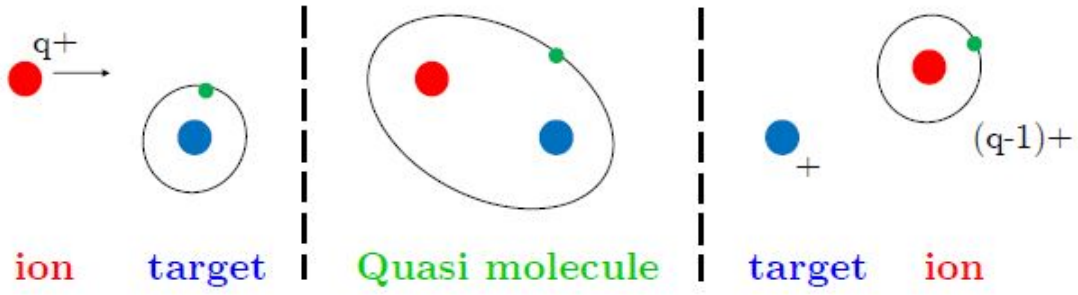

Figure 5: An illustration of a charge exchange process. In this thesis the ion is a He^{2+} ion and the target is a H_2 molecule. During charge exchange, one or more electrons are donated by the more negatively charged target to the positively charged ion. Temporarily a quasi molecule is formed from the ion and the target. This quasi molecule then breaks apart again and one or more electrons have been transferred from the target to the ion. This interaction also changes the momentum of the particles, since some of the energy from the incoming particle is transferred to the donor particle.

The charge exchange interaction can create several different fragment particles. For the particle interaction between He^{2+} ions and H_2 molecules, the following particles are possible to emerge after charge exchange: He^+, He, H_2^+ and H^+.

3 Experimental Setup

For the experiments with charge exchange and stopping, we operate the ZERNIKELEIF facility: a low energy ion accelerator facility. This facility consists of: ECRIS, the 110° bending magnet, the beamline, the 45° bending magnet and CHEOPS. A representative figure of the layout of ZERNIKELEIF is given in fig. 6.

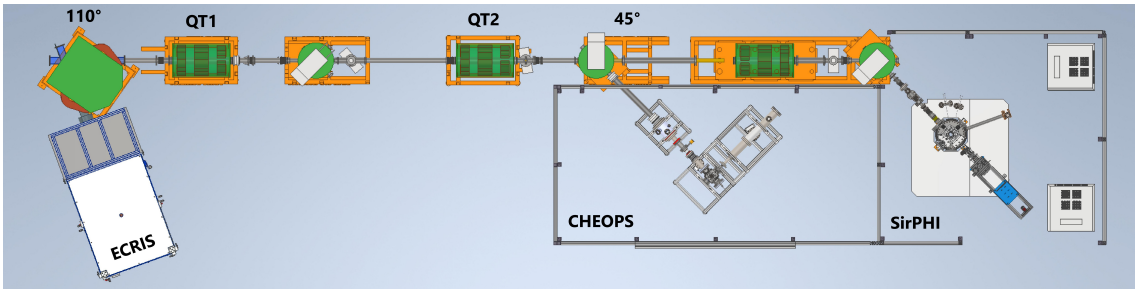

Figure 6: ZERNIKELEIF. An experiment starts with the ion source on the left where the ions are produced(white square) and then the particles travel trough the 110° bending magnet, followed by two triplets. Then the 45° bending magnet bends the particle towards CHEOPS (First cage from the left) where the RFA is mounted at the back. Shown with permission of M. Salverda

The experiment works by creating an ion at the source,which is then pulled out by the puller of the source towards the 110° bending magnet. Here the ion is transported towards the beamline. To optimize the source, an additional Faraday cup is added before the first triplet magnets (QT1). After the source has been optimized, the Faraday cup is removed out of the path of the beam and the ions travel further down the beamline. Here the ions come across a 45° bending magnet that in this case sends the ions towards CHEOPS. Here the beam can once again be optimized with the use of triplets and einzel lenses that focus the beam further. Lastly, the now focused and optimized beam can be used to perform experiments in CHEOPS.

3.1 Ion source (ECRIS)

ECRIS is an abbreviation for: Electronic Cyclotron Resonance Ion Source. The source works by energizing electrons which are heated by Radio Frequency (RF) radiation which in turn knock off electrons from the vaporized sample or gas that is present in the chamber and creates ions. In the source is a tin oven present that heats the tin to produce a tin vapor. An RF source with a frequency of 14 GHz is used to energise the electrons in the chamber that gyrate at 14 GHz around specific field lines generated by a permanent hexapole magnet of approximately 1T. When certain electrons have a higher kinetic energy than the ionisation energy of the sample, a plasma can be generated. This plasma is then used as a source of ions for experiments. With the use of a puller or einzel lens, the ions can be transported towards the 110° bending magnet. The puller is an electrode that can be put on a certain (negative) voltage to slightly tune the electric field that extracts the ions from the plasma. The einzel lens is a set of 3 electrodes of which the central one can be put on a negative or positive bias to focus the beam of ions originating from the plasma in the source. An overview of the Ion source is given in fig. 7.

Figure 7: An overview of the ion source used in the experiments. The blue cylinder is a 1T magnet, for plasma confinement. The ions leave the magnet on the left side of the magnet (viewed from the image on the left).

3.2 110° Bending magnet

When a plasma is generated from a pure sample of tin, all of the different isotopes of tin will be present in this plasma. To be certain we only use one type of isotope of tin, the mass-over-charge ratio of the tin plasma is used to separate the different isotopes. Here the 110° bending magnet comes into play. This bending magnet consists of thick copper coils, which produce a magnetic field that can change the direction of the beam envelope. The magnetic field strength can be controlled with a computer. When a sweep of the current is then performed, the mass-over-charge spectrum of ions from the source can be obtained from reading out the beam current at the first Faraday cup as a function of the current provided to the 110° bending magnet. An image of the 110° bending magnet is shown in fig. 8

Figure 8: An overview of the 110° bending magnet. The bending magnet is used to separate the different isotopes and charge states by making use of the mass-over-charge ratio of the different ions. By measuring the ion current at the first Faraday cup and compare it to the current provided to the magnet, the different ions can be separated and then send further down the beamline.

In this thesis, tin ions with the Sn-118 isotope and a charge state of 3+ are used instead of the more dominant Sn-120 isotope. This isotope is used to avoid confusion over which ion is actually being measured, since Ar-40 present in the air will have a contribution to the Sn-120 isotope peak. Instead the second most abundant isotope Sn-118 is used to overcome this problem and to know with certainty that only tin ions are measured in the experiments.

3.3 The beamline

Inside the beamline is a vacuum present that is held at a pressure of P < 1E-7 mBar. Due to this pressure ions can travel down the beamline without encountering air particles which will disperse the ions to the point where no ions are able to travel to the Faraday cup. Once an ion beam has been generated and the right isotope has been selected, the beam can be transported through the beamline. The first Faraday cup therefore has to be retracted from the center of the beamline and several valves have to be opened for the beam to be able to enter the rest of the beamline. In the beamline, the ions encounter two triplet magnets. A triplet is a set of three quadrupole magnets in parallel orientation relative to each other, that can focus the ions beam. The magnets are controlled via a set of potentiometers that can very accurately, i.e. ∼0.01% resolution, control the current to the different sets of magnets of the triplet. Images of the first Faraday cup and the first triplet are shown in fig. 9.

Figure 9: An overview of the first Faraday cup(left image) and the first triplet(right image). The Faraday cup can be lowered into the beamline to optimize the settings of the Ion Source, Puller and Einzel Lens before sending the ions further down the beamline. When the beam is optimized, the Faraday cup is then retracted from the beamline and the ions encounter the triplets. The triplets are then used to focus and steer the beam into the RFA at CHEOPS.

Once the ion beam exits the triplets, it travels further down the beamline until the beam reaches the 45° bending magnet.

3.4 45° Bending magnet

The 45° bending magnet performs just like the 110° bending magnet, except for the bending angle. The magnet can bend an ion beam 45° towards the right experiment. In this particular case we use the 45° bending magnet that steers the ion beam towards the CHEOPS experiment. This is done with the help of the large electromagnetic coils present in the device, that are controlled via a computer. A figure of the 45° bending magnet is given in fig. 10.

Figure 10: An overview of the 45° bending magnet. The ions enter the magnet from the right side of the image and are then bended 45° with the use of electromagnets, which are controlled at the source to steer the ions into the RFA.

3.5 Chopper Sweeper

The Chopper Sweeper is a device that can produce a discretized ion beam from a continuous ion beam. By sweeping the beam over a diaphragm. This device consists of 2 metal plates that switch polarity in a certain time interval to create pulses of ions or 'sweeps'. This gives the operator the possibility to locate the time as the starting time for a certain experiment as the current readout is now effectively switched from continuous readout to a discretized readout. The switching happens at several thousand Hertz and the polarities of the plates are switched between -100 V and +100 V. However, this device is not used in the experiments performed in this thesis, but the incoming ions do travel through this device.

3.6 CHEOPS

The abbreviation CHEOPS stands for CHarge Exchange Observed by Particle Spectroscopy. It is the name for a range of experiments that can be performed with the use of this setup. When the beam enters the setup, the ions are once again focused by beam optics. CHEOPS can then be used to perform charge exchange on particles with the help of H_2 gas or D_2 gas that are injected into the chamber of CHEOPS through a thin capillary tube. Once charge exchange is performed, the particles can go in two directions. The ions continue to move in the forward direction towards the RFA and charged target fragments can be extracted perpendicular to the ion beam direction, towards the Time of Flight (ToF) spectrometer where the different masses of the fragments can be analyzed. This thesis only makes use of the RFA for obtaining data and hence omits the use of the ToF spectrometer. A cross section of CHEOPS is depicted in fig. 11.

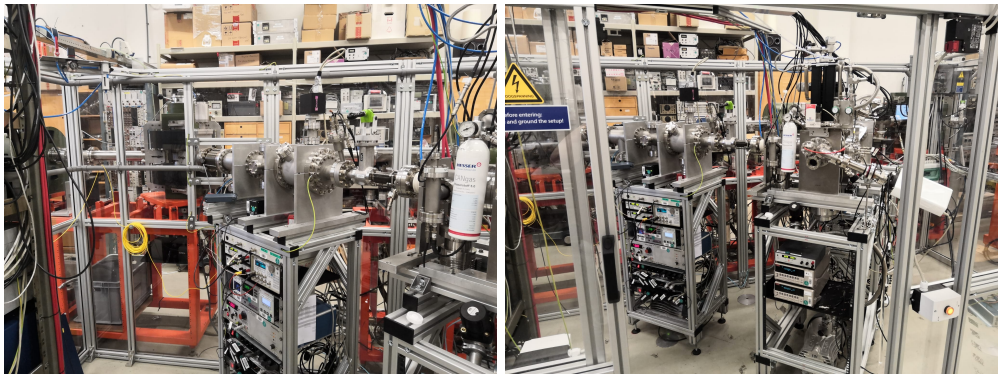

Figure 11: An overview of CHEOPS. The ions enter the setup from the back (left image) and then travel through the chopper to then reach the reaction chamber of CHEOPS, where the ions can potentially interact with a gas to exchange charges, to then impact on the Faraday cup of the RFA.

3.7 Retarding Field Analyzer

Understanding the working principles of the RFA is of great importance to this research. The RFA can be seen as an electrostatic measurement device to which different biases can be applied. The biases can be applied to several different grids inside the RFA. A figure of the particular RFA (Kimball FC-73A) [13] used is depicted in fig. 12.

Figure 12: Left: The topside of the RFA. The inputs on top of the RFA from left to right are: The retarding grid voltage, the current readout, the suppressor grid voltage. Right: The backside of the RFA. The shield is clearly visible in the middle of the flange. The hole in the middle is where the positive ions enter the RFA.

An ion will either hit the shield or enter the hole in the middle of the backside of the RFA. When an ion enters the RFA, it will first encounter a grounding grid that is hard grounded with the setup, see fig. 13. Ions and electrons that are out of focus, can hit the grid plate and are neutralized. The remaining ions now encounter the retarding grids. Here a voltage between 0 V and 5000 V can be applied. In this particular setup the maximum voltage that can be applied is 4500 V, a higher voltage causes arcing within the RFA. This arcing is undesirable, because it sends a high voltage over the ground wire, which can have a negative impact on other measuring devices. A voltage in the aforementioned range can stop an ion beam if the total beam energy is equal to q times the voltage applied to the retarding grid, with q being the charge state of the ion. An ion that travels through this grid 'feels' the electric field of the grids and is influenced by it due to the positive potential applied. If an ion is able to travel through the retarding grids, it encounters the suppressor grid. The suppressor grid's function is to repel any secondary electrons that emerged after an interaction from a positive ion with the Faraday cup. These secondary electrons are important to send back, otherwise a too high ion current would be measured. The suppressor grid also slightly acts as an

accelerator for the positive ions since there is an electric field between the retarding grids and the suppression grid. Lastly, when the ions pass through the suppressor grid, they enter the Faraday cup where they will impact the cup. This interaction generates a current which can then be measured using an ammeter. A schematic view of the RFA is depicted in fig. 13.

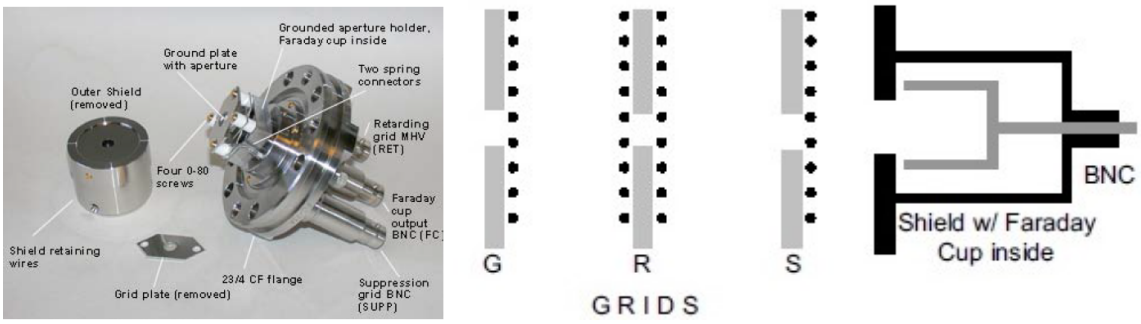

Figure 13: Left panel: The RFA taken apart. Here you can see the inner structure and workings of the RFA. Right panel: A schematic view of the RFA. From left to right: Grounding grid (G), Retarding grids (R), Suppressor grid (S). Image taken from [13].

4 Results

Over the course of several weeks, multiple measurements were performed using an RFA. Most of all the determination of transmission spectra for different ions were measured. Furthermore, the Ion Energy Distribution Functions (IEDF) were then derived from these transmission functions. The results of these measurements are shown and enlightened upon in the subsections hereafter.

4.1 H^+ Experiments

The results regarding the hydrogen measurements are presented first. These measurements were performed on the 30^{th} of March 2022 and consist of an RFA transmission spectrum measurement between 0 V - 4200 V with a step size of 40 V. The results of this experiment are depicted in fig. 14.

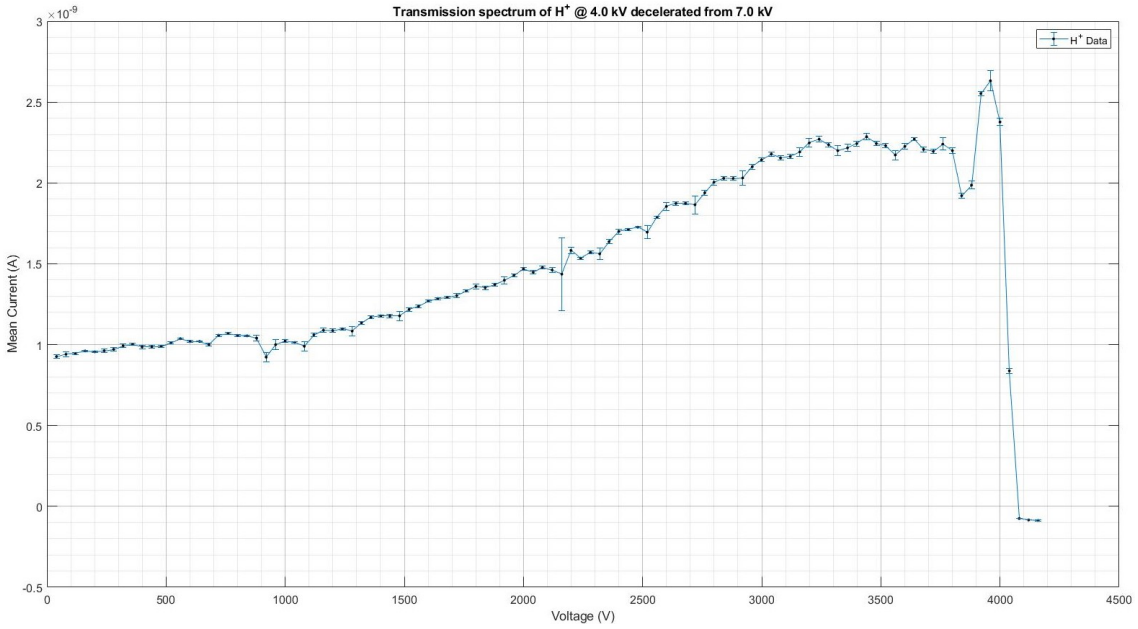

Figure 14: The RFA transmission spectrum of 4 keV H^+ by putting a retarding potential on the RFA grids from 0 V - 4200 V, with a step size of 40 V. The transmission increases as a function of the voltage and right before 4000 V sharply decreases and increases again and then drops off to zero current.

Afterwards another ion spectrum measurement was performed, but now between 3900 V - 4200 V with a step size of 5 V. The results of the experiment are presented in fig. 15.

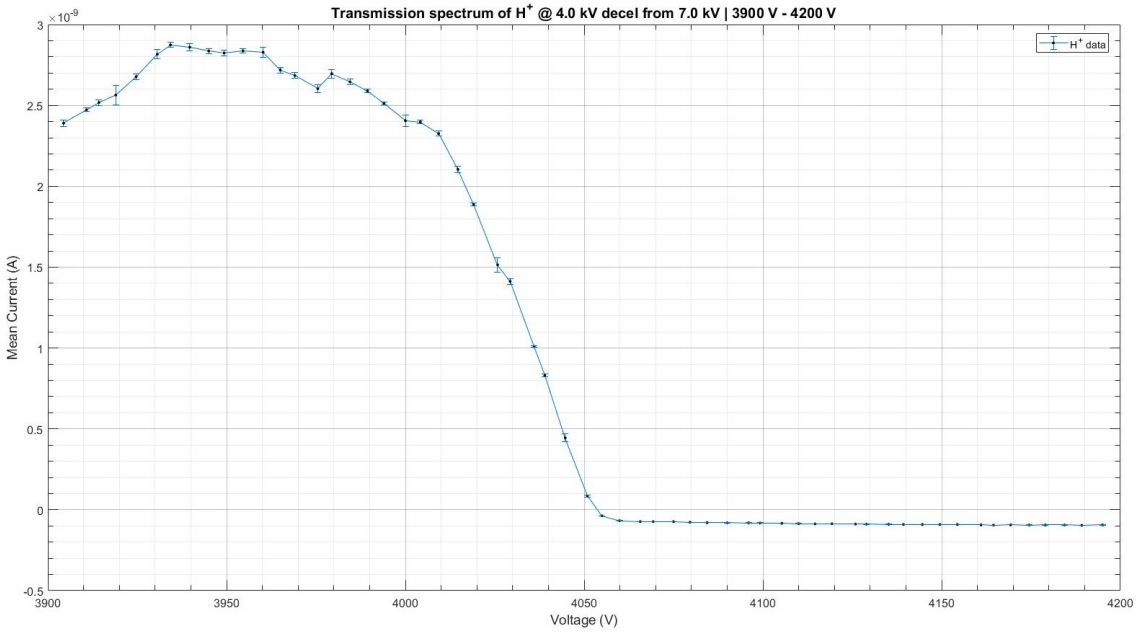

Figure 15: The ion spectrum of H^+ with a retarding voltage on the grids between 3900 V - 4200 V and a step size of 5 V. Here the drop off is very well defined and from this data the resolution can be determined.

From the data from this last figure, one can then perform a derivation on the data points, to obtain information on the ion beam properties. The results of this derivation are shown in fig. 16.

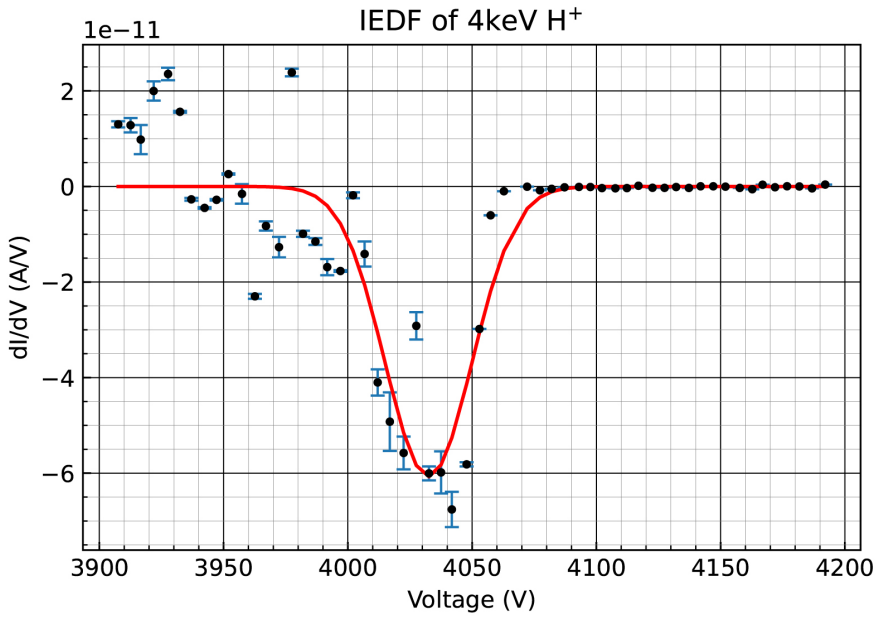

Figure 16: The differentiated data of H^+ ions between 3900 V - 4200 V, with a step size of 5 V. A Gaussian distribution has been fitted to the data points as the data suggested. The data points before about 3750 V are not relevant, because all ions pass the retarding grids.

From the fitting in python, we obtain that the $\sigma = 17.5 \pm 1.7$ V . Therefore the Full Width Half Max (FWHM) $= 2.35 \cdot \sigma = 41.1 \pm 4.0$ V. If we divide this number by the point where we expect the drop off to take place (i.e. 4000 V), we can asses an estimate of the energy resolution.

$$\left(\frac{41.1022278}{4000} \pm \frac{41.1022278}{4000} \cdot \sqrt{\left(\frac{4.0430090}{41.1022278} \right)^2 + \left(\frac{1}{4000} \right)^2} \right) \cdot 100 \approx 1.03 \pm 0.10\% \tag{4.1}$$

4.2 He^{2+} Experiments

The results of the Helium experiments are presented in this subsection. These measurements were performed on the 31^{st} of March 2022. There is a difference in measurements, one measurement is performed without the presence of hydrogen gas and one measurement is performed with the presence of hydrogen gas (Charge Exchange). The RFA transmission spectrum measurements from 0 V - 4200 V with a step size of 40 V without gas are given in fig. 17.

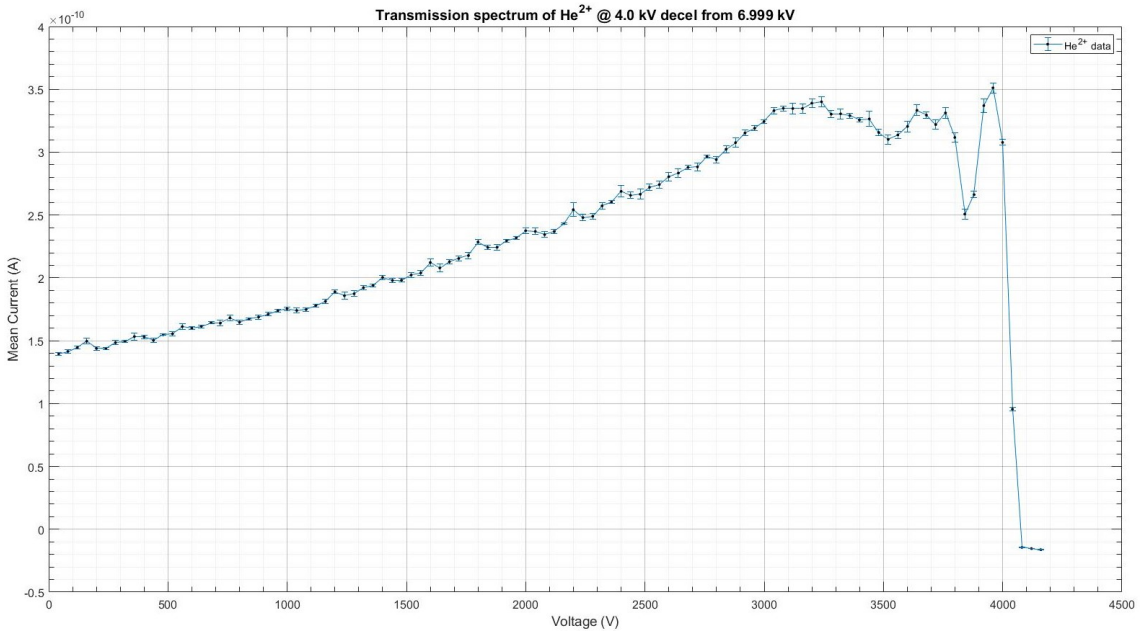

Figure 17: The ion spectrum of 8 keV He^{2+} by putting a retarding potential on the RFA grids from 0 V - 4200 V and a step size of 40 V. The transmission increases as a function of the voltage and right before 4000 V sharply decreases and increases again and then drops off to zero current.

Furthermore, measurements of the RFA transmission spectrum were repeated however now the range was from 3900 V - 4100 V with a step size of 5 V. The results are given in fig. 18.

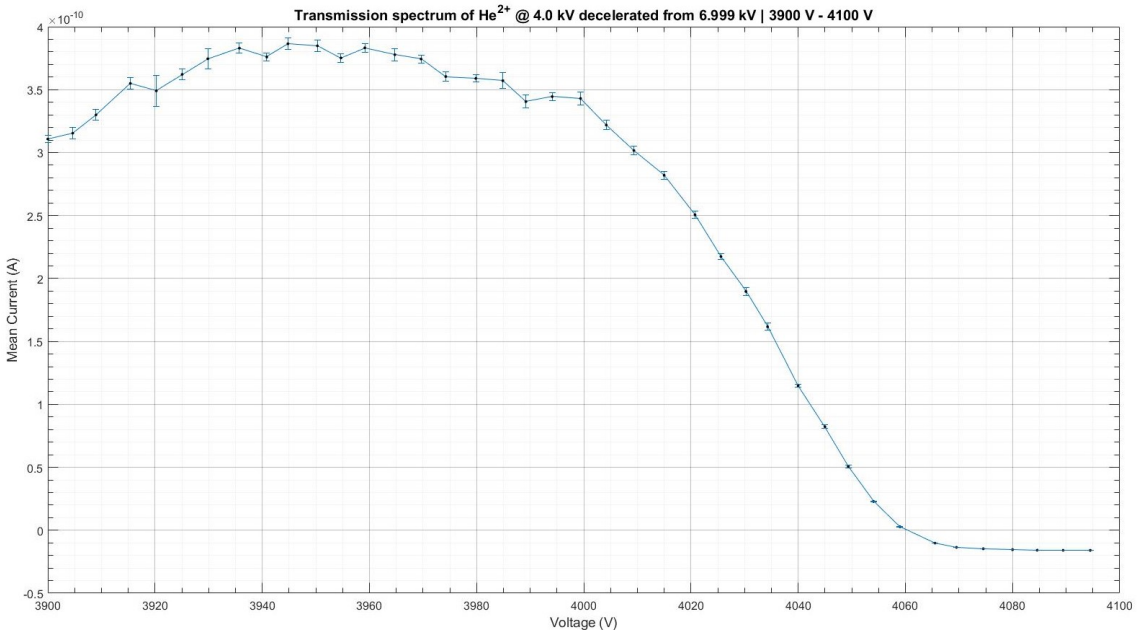

Figure 18: The RFA transmission spectrum of 8 keV He^{2+} with a retarding voltage on the grids between 3900 V - 4100 V and a step size of 5 V.

From this last figure, one can then perform a derivation on the data points, to obtain the areas of large deviations. The results of this derivation are shown in fig. 19.

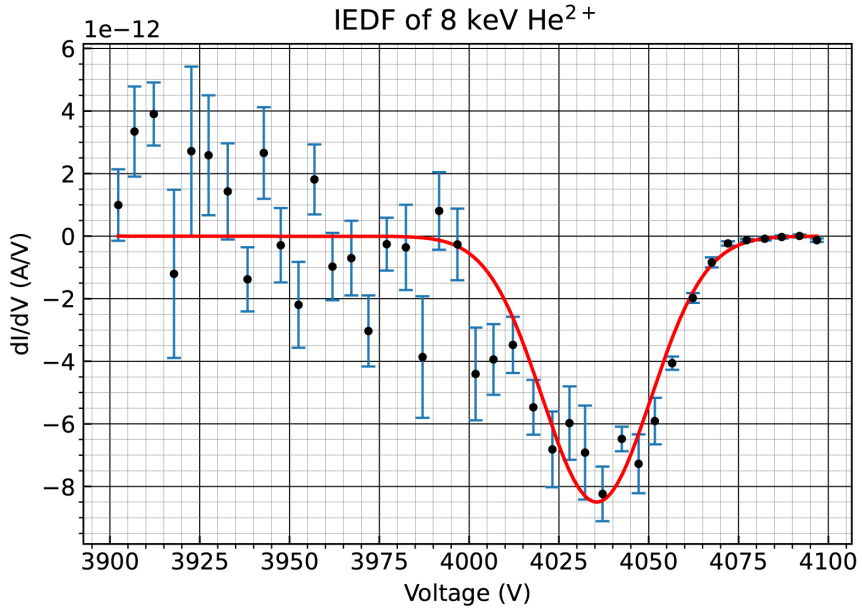

Figure 19: The differentiated data of He^{2+} ions between 3900 V - 4100 V and a step size of 5 V. A Gaussian distribution has been fitted to the data points.

From the fitting in python, we obtain that the $\sigma = 21.5 \pm 1.0$ V . Therefore the FWHM $= 2.35 \cdot \sigma$ $= 50.4 \pm 2.5$ V. If we divide this number by the point where we expect the drop off to take place (i.e. 4000 V), we can asses an estimate of the energy resolution.

$$\left(\frac{50.4419570}{4000} \pm \frac{50.4419570}{4000} \cdot \sqrt{\left(\frac{2.4535871}{50.4419570} \right)^2 + \left(\frac{1}{4000} \right)^2} \right) \cdot 100 \approx 1.26 \pm 0.06\% \tag{4.2}$$

4.2.1 He^{2+} CX Experiments

Here the results of 4 keV He^{2+} experiments with hydrogen gas present in the collision chamber and first charge exchange results are presented. These measurements were performed on 31^{st} of March 2022. During these measurements a constant flow of 1 ml min^{-1} of H_2 gas was injected into CHEOPS. In these experiments the charge exchange from He^{2+} to He^{+} has been measured with the RFA. The results of these measurements are shown in fig. 20.

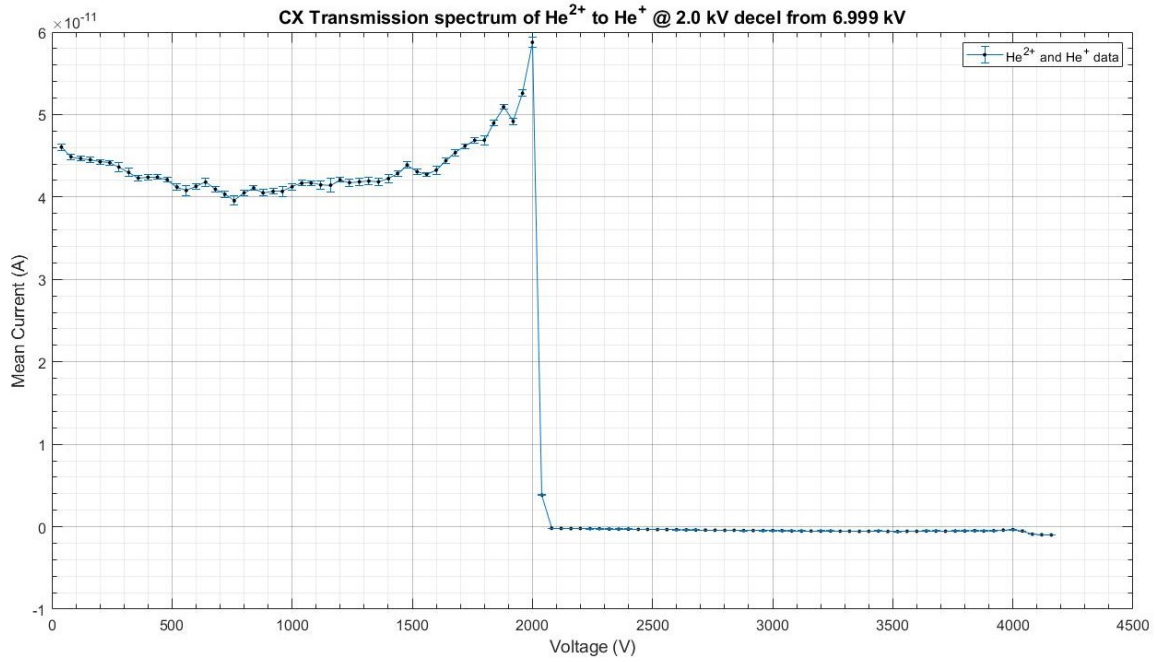

Figure 20: The RFA transmission spectrum of the He^{2+} and He^{+} ions under the influence of H_2 gas from 0 V - 4200 V and with a step size of 40 V. This spectrum differs from the spectra without H_2 gas, because here the mean current first decreases until about 750 V and then increases until about 2000 V, at which point the He^{2+} ions are blocked by the RFA and the RFA only lets the He^{+} ions pass.

Once we zoom in on the figure, we can see the amount of He^+ that emerged from charge exchange with the H_2 gas. This is shown in fig. 21.

Figure 21: The He^+ part of the 0 V - 4200 V figure. The same pattern as in fig. 20 seems to have been followed. The current first decreases until about 3500 V, after which the current increases again until about 4000 V and then drops off to zero current.

From this last zoomed in figure, one can then perform a derivation on the data points, to obtain the areas of large deviations. The results of this derivation are shown in fig. 22.

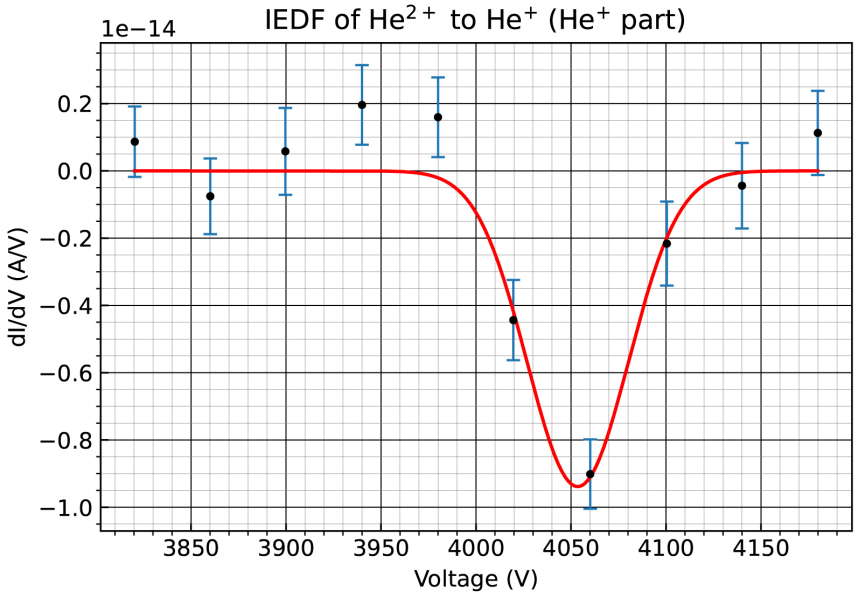

Figure 22: The differentiated He^+ data from 3800 V - 4200 V and with a step size of 40 V. A Gaussian distribution has been fitted to the data as the data suggested.

From the fitting in python, we obtain that the $\sigma = 37.6 \pm 6.01$ V . Therefore the FWHM $= 2.35 \cdot \sigma = 88.4 \pm 14.1$ V for the He^+ ions produced by charge exchange. If we divide this number by the point where we expect the drop off to take place (i.e. 4000 V) and we perform error analysis, we get:

$$\left(\frac{88.4263565}{4000} \pm \frac{88.4263565}{4000} \cdot \sqrt{\left(\frac{14.1135445}{88.4263565} \right)^2 + \left(\frac{1}{4000} \right)^2} \right) \cdot 100 \approx 2.21 \pm 0.35\% \tag{4.3}$$

Now when the weighted average current of both ions is calculated, one can calculate what percentage of Helium ions have exchanged their charge with H_2 gas. A representative illustration is given in fig. 23.

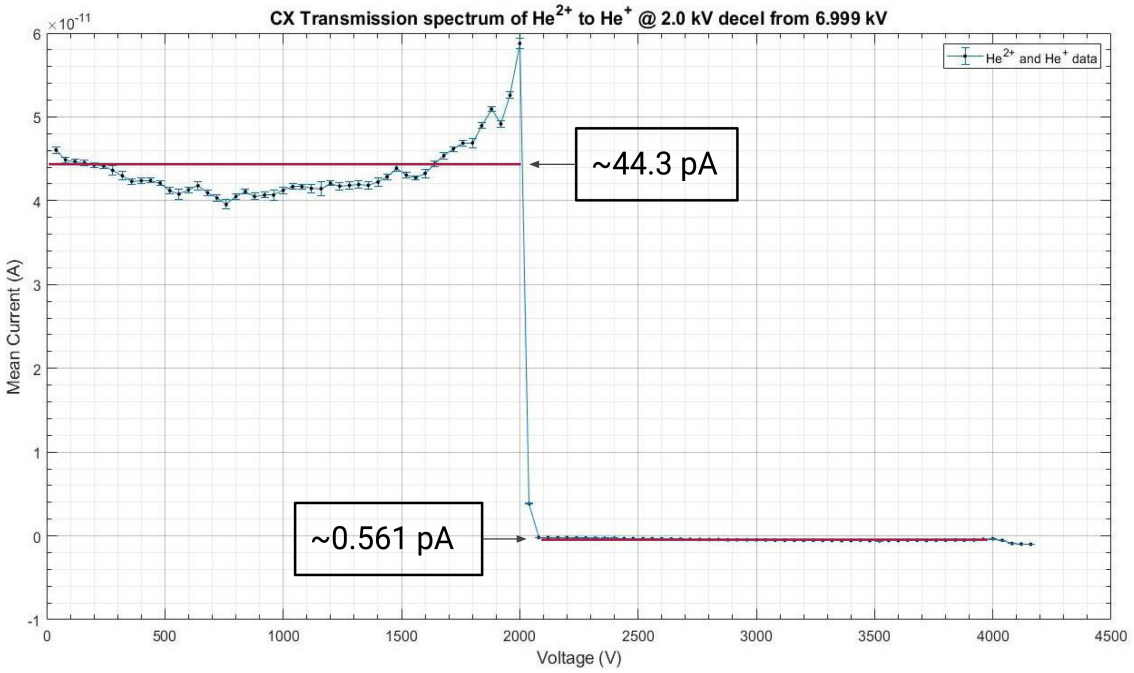

Figure 23: The ion spectra of the He^{2+} and He^+ ions under the influence of H_2 gas from 0 V - 4200 V and a step size of 40 V. In the figure, lines are plotted with the approximate average mean current. This is to indicate how the calculation of eq. (4.4) *came about.*

It was found that the average current for the He^{2+} was 44.3 ± 0.05 pA and the average current for He^+ was 5.61 ± 0.04 pA. The calculation is given in eq. (4.4).

$$\left(\frac{2 \cdot 0.5614367}{44.34440} \pm \frac{2 \cdot 0.5614367}{44.34440} \cdot \sqrt{\left(\frac{1}{2} \cdot \left(\frac{0.05253407}{44.34440} \right) \right)^2 + \left(\frac{0.004326599}{0.5614367} \right)^2} \right) \cdot 100 \tag{4.4}$$

$$\approx 2.53 \pm 0.02\%$$

Thus $2.53 \pm 0.02\%$ of the He^{2+} ions have undergone charge exchange to He^+.

4.3 Sn^{3+} Experiments

In this subsection we explore the results of the RFA transmission spectrum of 12 keV Sn^{3+} ions. These measurements were performed without the presence of H_2 gas on the 29^{th} of March 2022. The results are shown in fig. 24.

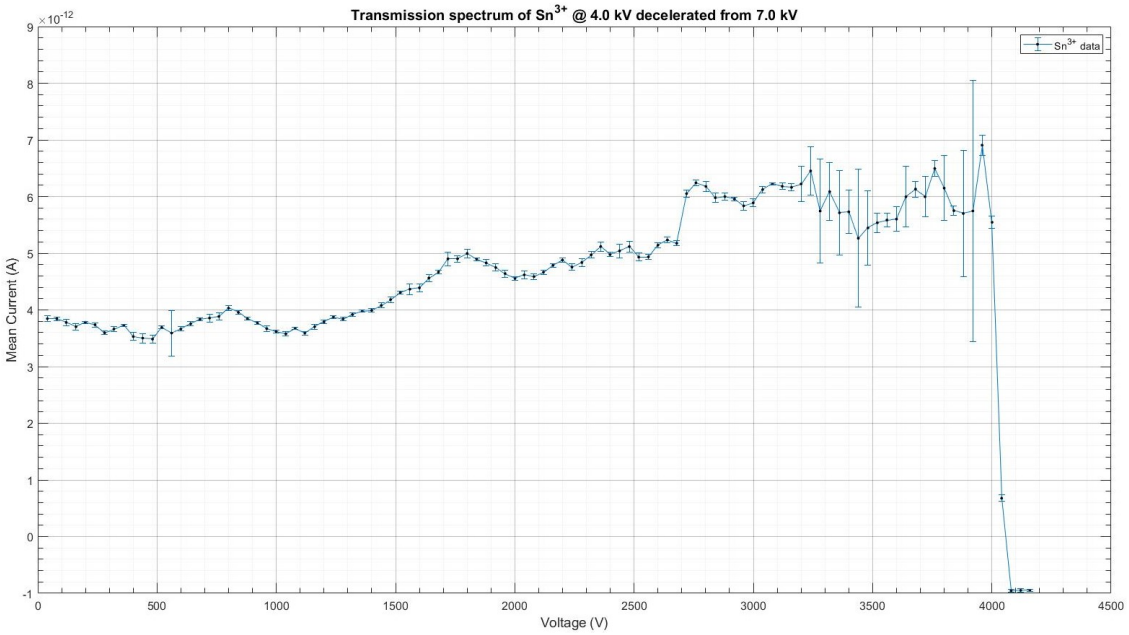

Figure 24: The RFA transmission spectrum of Sn^{3+} by putting a retarding potential on the RFA grids from 0 V - 4200 V. The transmission increases as a function of the voltage and decreases right before 4000 V and then drops off to zero current. Due to unknown reasons, the data from 3100 V - 3900 V shows large uncertainties.

Furthermore, measurements of the RFA transmission spectrum were repeated however now the range was from 3900 V - 4100 V with a step size of 5 V. The RFA transmission spectrum is given in fig. 25.

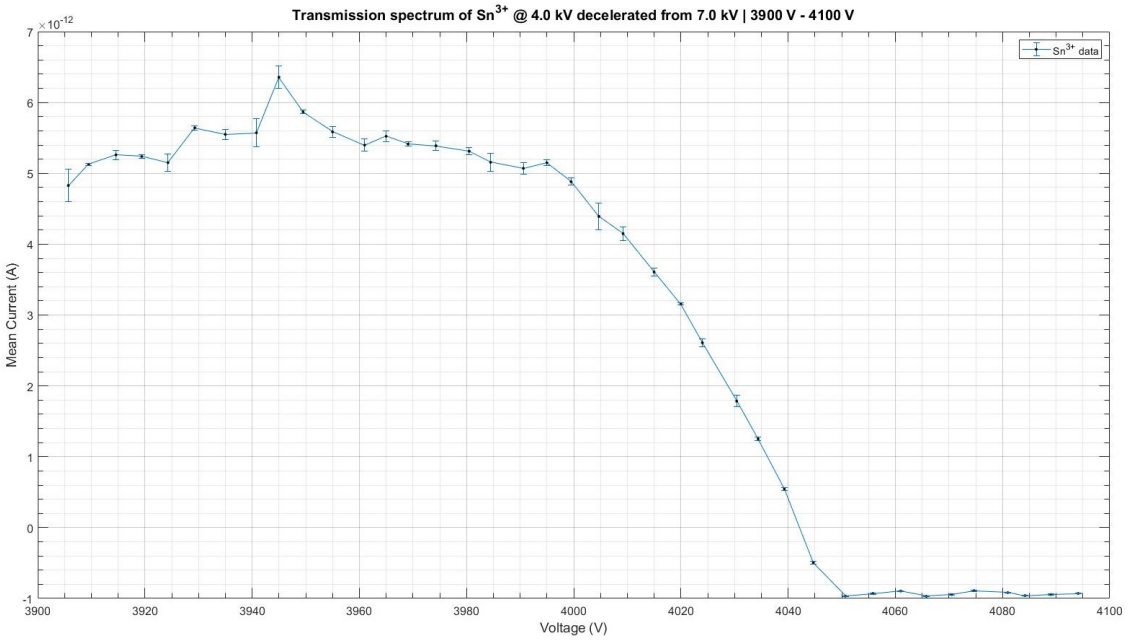

Figure 25: The ion spectrum of Sn^{3+} with a retarding voltage on the grids between 3900 V - 4100 V and a step size of 5 V. Here the drop off is very well defined and from this data the resolution can be determined.

From this last figure, one can then perform a derivation on the data points. The results of this derivation are shown in fig. 26.

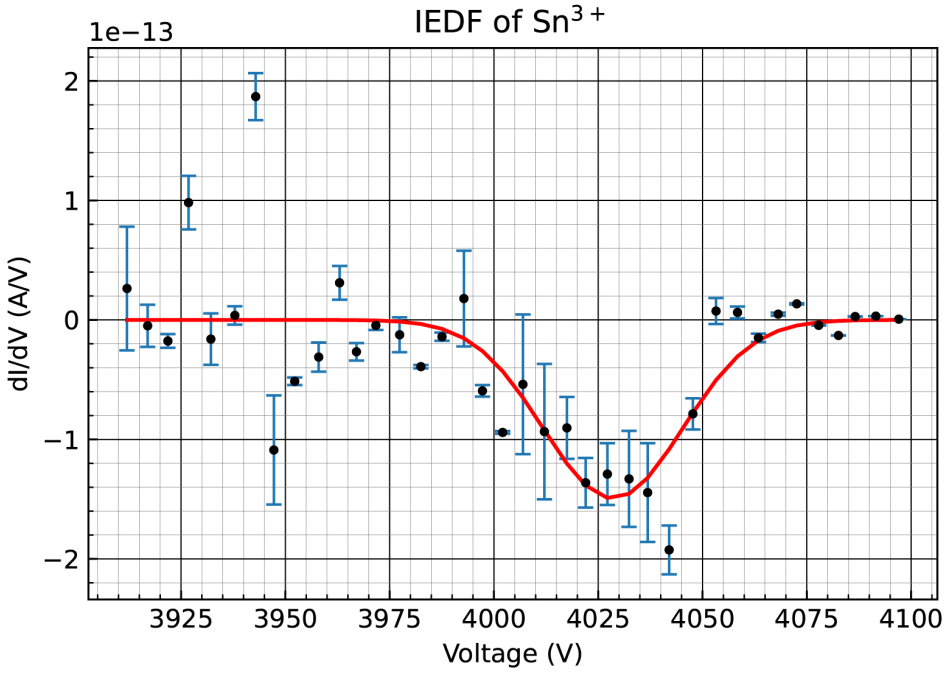

Figure 26: The differentiated data of Sn^{3+} ions between 3900 V - 4100 V, with a step size of 5 V. A Gaussian distribution has been fitted to the data points as the data suggested.

From the fitting in python (SciPy module), we obtain that $\sigma = 16.7 \pm 3.18$ V . Therefore the FWHM $= 2.35 \cdot \sigma = 39.3 \pm 7.47$ V. If we divide this number by the point where we expect the drop off to take place (i.e. 4000 V) and we perform error analysis, we get:

$$\left(\frac{39.3356017}{4000} \pm \frac{39.3356017}{4000} \cdot \sqrt{\left(\frac{7.4732874}{39.3356017} \right)^2 + \left(\frac{1}{4000} \right)^2} \right) \cdot 100 \approx 0.98 \pm 0.19\% \tag{4.5}$$

4.4 Comparison of the different ions

When one plots all the data for the different ions in one graph, a trend emerges. The trend that emerges shows that the transmission spectra for the different ions are in good agreement with each other. The results are shown in fig. 27

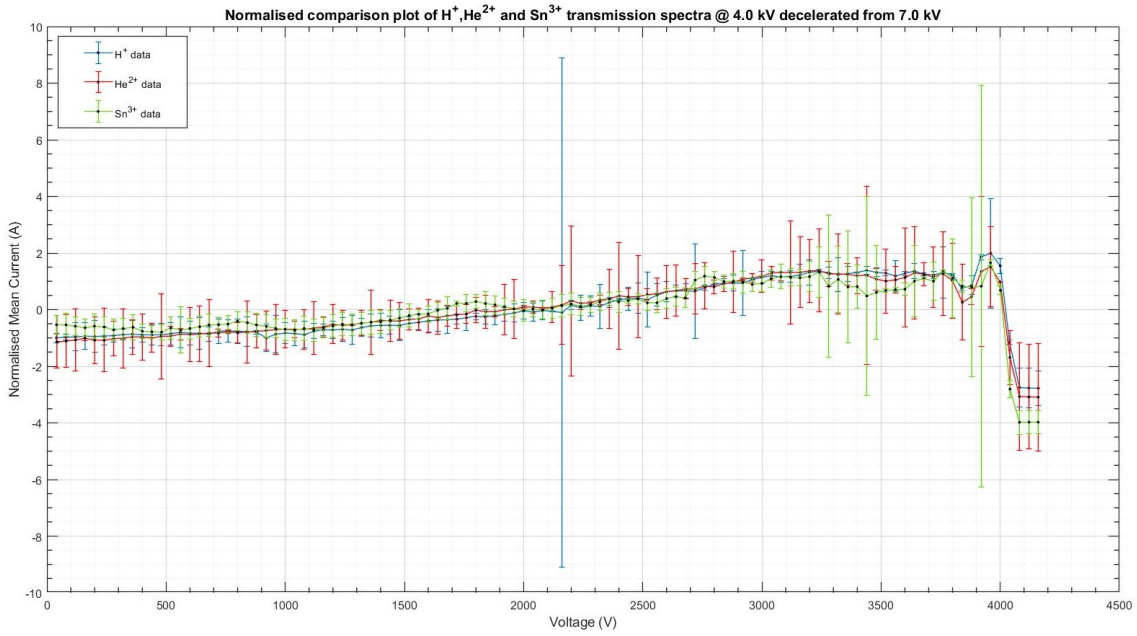

Figure 27: The different ion spectra of the 4 keV H^+, 8 keV He^{2+} and 12 keV Sn^{3+} ions in one figure. The mean current in the plot is normalised to show that the different trend data are in good agreement, as the error bars of the different data coincide with each other.

From fig. 27 we can see that shape of the transmission spectra is in close agreement for the different ions, even though the data of the He^{2+} and Sn^{3+} ions contain more uncertainties than the H^+ ion.

5 Discussion

In this thesis we explored the RFA transmission spectra and IEDF's of different mono-energetic ions as a function of the retarding voltage. Extensive literature research is missing in this area of expertise, hence these results are expanding our horizons. There was a graph provided by the manufacturer of our RFA [13], that had much of the same characteristics as the 3900 V - 4100 V graphs in this thesis. However, their experiments were performed with electrons and at relatively low voltages.

The H^+ experiments in section 4.1 shows the different experiments that were performed. The first experiment shows the mean current as a function of the retarding voltage (fig. 14). The overall trend of fig. 14 shows an increase in the current as the voltage increases, until it reaches a retarding voltage of around 3000 V. After this threshold the current stays more or less stable until about 3800 V. After 3800 V the current first decreases rapidly and then increases sharply, following the drop down to 0 V since then all the ions are blocked by the RFA. The lensing effect on the beam due to the electric potential on the grid is the most likely reason for this behaviour as demonstrated in fig. 3. Moreover we can see that due to the small mass of the proton, the ion is much more prone to instabilities in the beamline. This shows from the 'dips' along the spectrum. The large error bar at the data point at around 2200 V can be explained by a large sudden decrease in current. Since we were interested in the resolution of the RFA, we take more precise measurements between 3900 V and 4100 V with a step size of 5 V. The slope is now statistically more significant and differentiation was performed on the data points, resulting in fig. 16. Python (SciPy module) has been used to fit the best possible Gaussian function through the data points. A Gaussian function has been used to fit the data points, as the shape of the data suggested a Gaussian distribution and this result was moreover expected. Lastly, the data points before 3975 V bear no significance since we are only interested in the area where the drop off takes place. The resolution resulting from the calculation based on the FWHM of the Gaussian distribution shows that the resolution is close to 1%. This is a very peculiar result, as the theoretical solution of [6] suggest that the resolution of the RFA (albeit with three grids in their paper) can be no smaller than about 2%. The reason for this smaller resolution is outside the scope of this research but is very interesting to study further in the future.

The He^{2+} experiments in section 4.2 show very similar characteristics and spectra as the H^+ experiments. Here the mean current is measured as a function of the retarding voltage on the grids. We can notice that the mean current increases over time and becomes approximately constant at around 3000 V. The current suddenly drops and than sharply increases again close to 4000 V. This again is presumably caused by the lensing effect the grids have when the potential of the grids comes close to the potential of the ions. Once more the experiment was repeated for voltages ranging between 3900 V - 4100 V with a step size of 5 V. These settings were used to more precisely capture the behaviour of the drop off and thus determine the resolution again. From the FWHM of fig. 19 it was found that the resolution was around 1.3% once more further adding confidence to the 'true' resolution of the RFA. The points before 3975 V in fig. 19 bear little statistical significance, as these points originate from before the area of interest, i.e. before the drop off point).

The He^{2+} CX experiments or Charge eXchange experiments show a different spectrum than the previous experiments. This experiment involves the presence of H_2 gas in the reaction chamber in front of the RFA. To be able to perform a CX experiment, the potential energy had to be at about half of the maximum voltage that the RFA was able to handle, before the RFA started arcing. This happens at about 4500 V, so it was chosen that the maximum safe voltage was around 4200V. When examining the trend in fig. 20, it appears to be the case that the mean current first decreases before it increases until the 2000 V drop off point is reached. After this point, only the He^{2+} ions that reacted with the H_2 gas and became He^+ ions were able to traverse the grids. The He^+ spectrum is shown in the zoomed in part of fig. 20 in fig. 22. Here the same trend as in fig. 20 can be observed, where the current first decreases before it increases again. On the data from fig. 21, differentiation was performed to be able to calculate the resolution of the RFA after CX. This result can be

observed in fig. 22. The trend in this graph indicates a Gaussian distribution and has been fitted to the data points. From the FWHM of this distribution, the resolution was determined to be about 2.2%. However, more data points need to be measured between 3900 V - 4100 V to more accurately determine the FWHM of the distribution and calculate a more accurate resolution. Furthermore, the average mean current for the different ions between 0 V - 2000 V and 2000 V - 4100 V for He^{2+} and He^{+} were determined, respectively. This is illustrated in fig. 23. Once these average mean currents were determined, the percentage of He^{2+} ions that reacted with H_2 gas could be determined. From the calculations, it was shown that the percentage of ions that exchanged their charge was about 2.5%. This percentage seems to be in agreement with the expected percentage of charge exchange from cross-section measurements at the same H_2 gas flow. Interestingly, the resolution calculated from the He^{+} ions in fig. 22, is within the error of the percentage of ions that have undergone charge exchange from He^{2+} to He^{+}. The significance of this coincidence is unknown at current times and should be investigated further in the future.

The Sn^{3+} experiments were performed and show a similar spectrum to the H^{+} and He^{2+} experiments. in fig. 24, The mean current first increases to about 2750 V after which the current seems to be stable until about 3200 V. After this point the beam is very unstable, resulting in large uncertainties. There is thus great instability in the area between 3200 V and 4000 V. The most likely reason for this behaviour is that the lensing effect is very strong in this range and since the beam current was relatively low during this measurement, it might be the case that the ions where dispersed greatly after traversing the retarding grids and therefore spread more throughout the Faraday cup resulting in the large uncertainties. The measurements have been repeated for voltages in the range of 3900 V - 4100 V with a step size of 5 V and is shown in fig. 25. The large uncertainties in fig. 24 appear to have disappeared. The data from this figure was then used to fit a Gaussian distribution to. From the FWHM of the distribution, it was calculated that the resolution was about 1%. Note that the resolution calculated in the H^{+} experiment lies within the same error as the resolution from this experiment. This provides further evidence that the 'true' resolution of the RFA is around 1%.

Lastly, the different transmission spectra are plotted in the same figure in fig. 27. This figure shows that when the transmission spectra are normalised w.r.t. the mean current, the transmission spectra are in close agreement even though the ions that are used differ significantly in material properties.

6 Conclusion

The aim of this thesis was to answer the question whether or not compact retarding field analyzers could be used to measure ion energy distributions. It has been demonstrated that it is possible to measure the IEDF's of different ions. It was found that the resolution from the 4 keV H^+ experiments was 1.03 ± 0,10%. From the 8 keV He^{2+} experiments it was found that resolution was 1.26 ± 0.06%. From the 8 keV He^{2+} CX experiments it was found that the 8 keV He^+ part of the data showed a resolution of 2.21 ± 0.35%, however more data is needed to more accurately determine the resolution. From the average mean current of the He^{2+} and He^+ data, it was determined that 2.53 ± 0.02% of He^{2+} ions have undergone charge exchange with H_2 gas. This result lies within the order of magnitude that is expected from cross-section measurements that were performed with the RFA. The resolution of the RFA was once more determined using the data from the 12 keV Sn^{3+} experiments, yielding a resolution of 0.98 ± 0.19%. This result is in great agreement with the resolution found in the 4 keV H^+ and 8 keV He^{2+} experiments. The 8 keV He^+ resolution appears larger which might be due to the fact that the He^+ ions were produced by charge exchange. In the charge exchange collisions energy is transferred which broadens the energy distribution. A wider energy distribution leads to an apparent worsening of the resolution. Lastly, when all the transmission spectra are plotted relative to each other it can be observed that the transmission spectra are nearly identical to each other, which means that the ions follow the potential landscape of the retarding grids in a very similar way despite having different material properties.

7 Outlook

During the research it was observed that the current was approximately constant between 3000 V and 3800 V for the different ions. However, their relative level to the peak current was different for each ion. This raises the question if this 'plateau' of constant current with respect to the peak current, depends on the charge state of the ion. An illustration of the behaviour in question is shown in fig. 28.

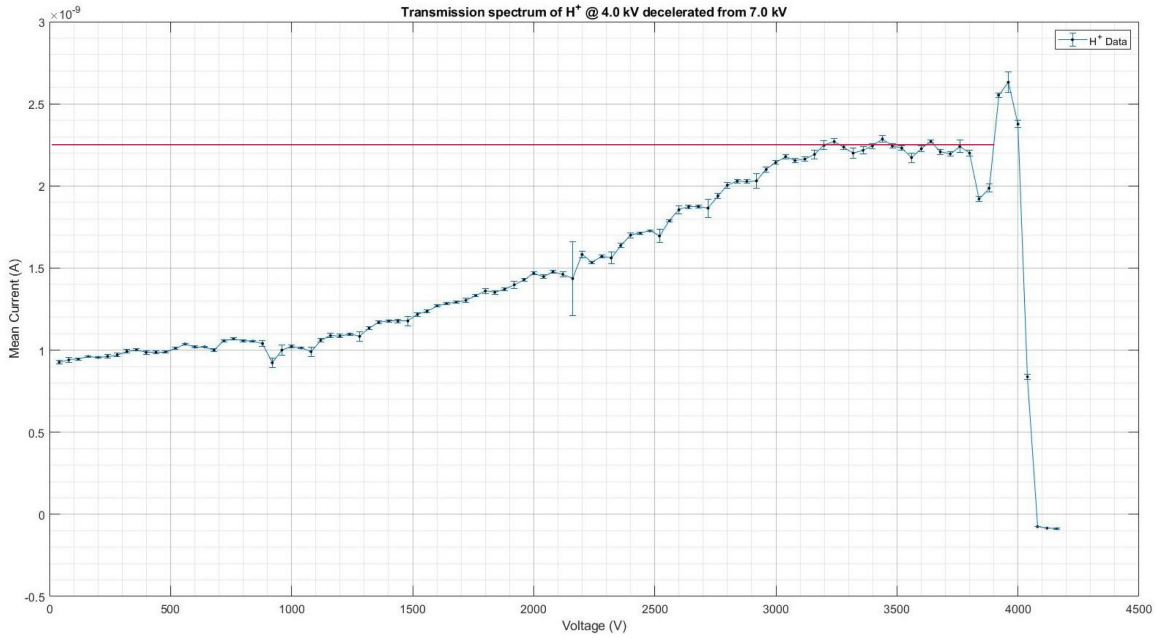

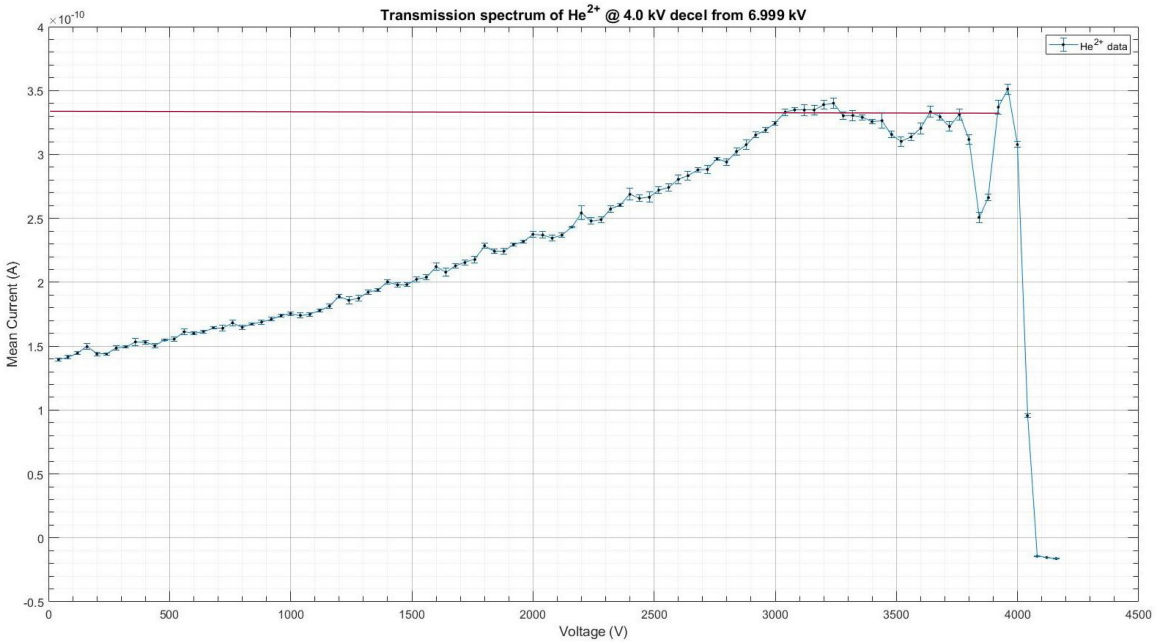

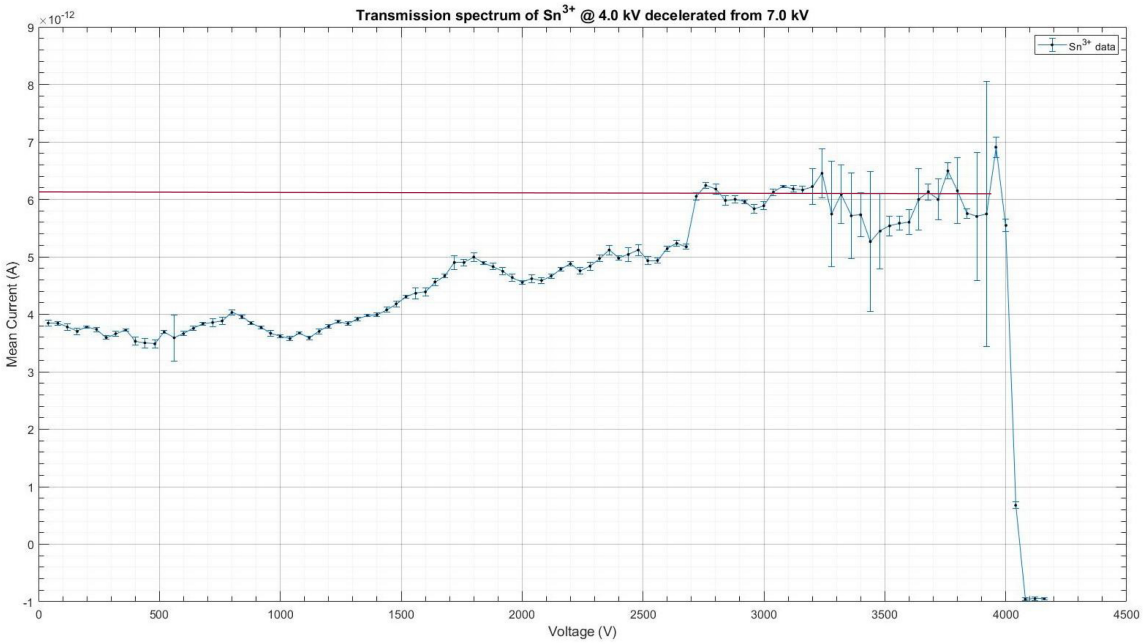

Figure 28: The different transmission spectra of the 4 keV H^+, 8 keV He^{2+} and 12 keV Sn^{3+} ions in separate figures. The different figures have lines plotted in them that indicate the approximate position of the current 'plateau' that might indicate the charge state of the particle.

If this 'plateau' with respect to the peak is dependent on the charge state, the RFA could be used as a detector for unknown charge states. As long as the operator is certain there is only one type of ion present in the experiment. In order to determine if the 'plateau' really depends on the charge state, an experiment should be constructed where the ion is the same but its charge state is altered. The data suggests that this can be done best with relatively low mass ions with the ability to have several different charge states. An ion with at least 3 different charge states would be advisable, to get a more statistically significant result.

Lastly, more data should be gathered for the more precise determination of the resolution from the 8 keV He^+ part of the data shown in fig. 21.

8 Acknowledgements

I would like to thank Ronnie Hoekstra, Klaas Bijlsma, Luc Assink, Subam Rai, Alex Kleinsmit, Mart Salverda, Ernst Lalkens and Boris Neijzen for their support and welcoming me into their group. Especially since everyone was always available for questions or to explain something. It was a very fun experience as I learned a lot from everyone of you. I would also like to thank Carla Olsthoorn for her support and help during the writing of this thesis.

9 Appendix

9.1 Error Analysis

To calculate the errors for the different values, an error analysis has been applied.

To calculate the resolution of the different ions and the RFA, the following equation was used:

$$\delta_{res} = \frac{A}{B} \cdot 100\% \tag{9.1}$$

The error could then be found via:

$$\Delta\delta_{res} = \delta_{res} \cdot \sqrt{(\frac{\Delta A}{A})^2 + (\frac{\Delta B}{B})^2} \tag{9.2}$$

Where δ_{res} is the mean resolution, ΔA and A is the error in the FWHM and the FWHM respectively of the best fit Gaussian distribution. ΔB and B are the error in the voltage and exact drop off point of the beam due to the retarding grids.

For the mean and error in the charge exchange percentage calculation (eq. (4.4)), a factor of 2 and $\frac{1}{2}$ have been added to compensate for the charge state of He^{2+}. This compensation was necessary, because the potential in volts is used instead of the potential in electron volts, such that the elementary charge was not involved in the calculation.

9.2 Data Acquisition

Data from the RFA was acquired with the use of the RFA Measurement program, developed by the Quantum Interactions and Structural Dynamics (QISD) Group from the University of Groningen with *Labview*^{TM} by National Instruments. The ion spectra figures have been made with $Matlab^{TM}$ by The Mathworks. The differentiated figures and Gaussian distributions have been made and fitted with Python (SciPy module) in *Google Colab*^{TM}.

10 References

[1] J. A. Fleming, *Instrument for converting alternating electric currents into continuous currents*, https://patentimages.storage.googleapis.com/23/09/50/6d4980acdfed12/US803684.pdf, Retrieved on May 2022, U. S. patent 803,684, (1905).

[2] "First transistor ieee milestone dedication", North Jersey Section of the Institute of Electrical and Electronics Engineers **56 (5)**, Retrieved on April 2022 (2009).

[3] C. T. Sah, "Characteristics of the metal-oxide-semiconductor transistors", IEEE Transactions on Electron Devices **11**, 7 (1964).

[4] G. E. Moore, "Cramming more components onto integrated circuits", Proceedings- IEEE **86(1)**, 82–85 (1998).

[5] ASML, *Euv lithography systems*, https://www.asml.com/en/products/euv-lithography-systems, Retrieved on May 2022, ASML, (2019).

[6] Y. Sakai and I. Katsumata, "An energy resolution formula of a three plane grids retarding field energy analyzer", Japanese Journal of Applied Physics **24(Part 1, No. 3)**, 337–341 (1985).

[7] T. H. M. van De Ven, V. Y. Banine, J. Beckers, C. A. De Meijere, R. M. van der Horst, and M. van Kampen, "Analysis of retarding field energy analyzer transmission by simulation of ion trajectories", Review of Scientific Instruments **89**, 4 (2018).

[8] R. A. Mapleton, *Theory of charge exchange (ser. wiley-interscience series in atomic and molecular collisional processes)*, Wiley-Interscience, (1972).

[9] R. Cabrera-Trujillo, "Hydrogen and helium charge exchange collisions at kiloelectronvolt energies: an electron–nuclear dynamics review", Plasma Sources Science and Technology **19**, 034006 (2010).

[10] R. Hoekstra, F. J. de Heer, and R. Morgenstern, "Photons shedding light upon basic charge exchange processes", Zeitschrift für Physik. D: Atoms Molecules and Clusters **21**, 81 (1991).

[11] S. D. Johnson, M. M. El-Gomati, and L. Enloe, "High-resolution retarding field analyzer", Journal of Vacuum Science and Technology B Microelectronics and Nanometer Structures **21**, 350–353 (2003).

[12] C. Böhm and J. Perrin, "Retarding-field analyzer for measurements of ion energy distributions and secondary electron emission coefficients in low-pressure radio frequency discharges", Review of Scientific Instruments **64(1)**, 31–44 (1993).

[13] *Fc-73a faraday cup*, Retrieved on May 2022, Kimball Physics, 2011.

[14] Z. Zhang, H. Tang, J. Cao, L. W. Y. Liang, Z. Chen, and J. Ren, "Measurement of the distribution of charge exchange ions in a hall-effect thruster plume", Plasma Sources Science and Technology **29**, 8 (2020).

[15] A. Holzner, *Magnetic field of an idealized quadrupole with forces*, Wikimedia Commons, 2012.